DNA supercoiling modulates eukaryotic transcription in a gene-orientation dependent manner

Ana Karina Morao[1,*], Almira Chervova[1], Yuya Zhao[2], Sevinc Ercan[2,*] and Germano Cecere[1,*]

[1]Mechanisms of Epigenetic Inheritance, Department of Developmental and Stem Cell Biology, Institut Pasteur, UMR 3738, CNRS, Paris 75015, France
[2]Department of Biology, Center for Genomics and Systems Biology, New York University, New York, NY 10003, USA

[*]Corresponding author ana.morao@pasteur.fr, se71@nyu.edu, germano.cecere@pasteur.fr

Key words: topoisomerases, DNA supercoiling, transcription regulation, *C. elegans*, histone modifications.

Summary

Transcription introduces torsional stress in the DNA fiber causing it to transition from a relaxed to a supercoiled state that can propagate across several kilobases and modulate the binding and activity of DNA-associated proteins. As a result, transcription at one locus has the potential to impact nearby transcription events. In this study, we asked how DNA supercoiling affects histone modifications and transcription of neighboring genes in the multicellular eukaryote *Caenorhabditis elegans*. We acutely depleted the two major topoisomerases and measured nascent transcription by Global Run-on sequencing (GRO-seq), RNA Polymerase II occupancy by ChIP-seq, gene expression by RNA-seq and four transcription-associated histone modifications by Cut & Tag. Depletion of topoisomerases I and II led to genome-wide changes in transcription dynamics, with minor disruptions to the histone modification landscape. Our results showed that *C. elegans* topoisomerase I is required for transcription elongation and is partially redundant with topoisomerase II. Analysis of transcription changes with respect to neighboring genes suggest that negative supercoiling promotes the transcription of genes with a divergent neighbor and positive supercoiling suppresses transcription of convergent genes. Additionally, topoisomerase depletion caused coordinated changes in the expression of divergent gene pairs, suggesting that negative supercoiling drives their synchronized expression. Conversely, the coordinated expression of convergent genes was disrupted, suggesting that excessive positive supercoiling inhibits transcription. Overall, our data supports a model in which DNA supercoiling generated by transcription at one site propagates along the eukaryotic chromatin fiber, influencing nearby transcription in an orientation-dependent manner.

Introduction

DNA templated processes including transcription and replication involve the opening of the double helix and the translocation of polymerases that force DNA to rotate around its axis. This rotation results in positively supercoiled DNA ahead of the polymerase and negatively supercoiled DNA behind[1]. Negative supercoiling at the promoter region contribute to strand separation and to the binding of the transcription machinery, while positive supercoiling can help destabilize nucleosomes for transcription progression[2–7]. On the other hand, an excess of DNA supercoiling has been shown to hinder transcription[8–10]. Therefore, the levels of DNA supercoiling need to be tightly regulated during transcription.

Transcription-induced supercoiling is resolved by the DNA cleavage and religation activity of topoisomerase enzymes. Type I topoisomerases resolve negative and positive supercoiling by cleavage, rotation and religation of one DNA strand. Type II topoisomerases cut both DNA strands, which allows them to resolve negative and positive supercoiling, as well as DNA catenates and knots[11]. Studies using topoisomerase mutants and inhibitors have provided key insights into how these enzymes influence gene expression[12]. RNA-seq and RNA Pol II binding analyses upon

single and double depletion of topoisomerases indicated that for the most part, topoisomerases I and II are redundant in the relaxation of transcription-induced supercoiling[9,13]. Some exceptions involving genes with high relaxation needs such as long genes have been reported in yeast and mammals[14,15]. Since mRNA and RNA Pol II binding report indirectly on transcription, methods that directly profile on-going transcription are required to fully understand the impact of topoisomerases on the transcription process.

In addition to affecting the transcription of the gene itself, the resulting supercoils can propagate to neighboring regions. Mapping of negative supercoiling using psoralen intercalation in yeast showed that transcription-induced supercoiling diffuses along the DNA fiber up to 1.5 Kb upstream of transcription start sites[16]. Modelling studies have proposed that this could affect transcription of neighboring genes, with divergent genes stimulating each other through the generation of negative supercoiling and convergent and tandem genes having inhibitory effect due to positive supercoiling[17–21]. Studies in bacteria using gene insertion in different orientations support this model[22–24].

In eukaryotes, *in vitro* experiments indicated that supercoiling can be absorbed by nucleosomes[25], thus the effect of neighboring genes might be buffered by chromatin. An initial study in yeast exploring the impact of DNA supercoiling on neighboring genes found that depletion of topoisomerase I and II inhibit the expression of genes located in close proximity regardless of their orientation[26]. Importantly, the authors used the auxin-inducible degron system for acute depletion, but high levels of basal degradation in the absence of auxin compounded the direct and indirect effects. Therefore, further research in eukaryotic models is required to understand how propagation of DNA supercoiling affects transcription in the context of chromatin, which has important implications for eukaryotic transcription since it may influence transcription of neighboring genes in organisms with small genomes and impact alternative transcription start sites in larger genomes.

In this study, we used acute depletion of the two main topoisomerases in *C. elegans* coupled with genomic approaches including nascent transcription profiling by Global Run-on sequencing (GRO-seq), ChIP-seq, RNA-seq and Cut & Tag, to investigate how DNA supercoiling impacts transcription and histone modifications with a focus on genes with different orientations. We found that topoisomerase I depletion disrupts transcription elongation, particularly for long genes, and this effect is increased with additional depletion of topoisomerase II. Depletion of topoisomerases increased transcription of genes with a divergent neighbor and inhibited transcription of convergent genes. Moreover, our results suggest that accumulation of negative DNA supercoiling at the promoter regions results in coordinated changes in the expression of divergent gene pairs. On the other hand, topoisomerases depletion perturbed the coordinated expression of convergent genes suggesting that too much positive supercoiling unbalances convergent transcription. While there were no global changes in the elongation-related histone

modification H3K36me3, and the heterochromatin mark H3K27me3, we observed a slight decrease in the promoter and enhancer associated modifications H3K4me3 and H3K27ac upon topoisomerase depletion. In summary, our results suggest that negative supercoiling promotes transcription of adjacent genes and contributes to their coordinated expression whereas positive supercoiling breaks synchronized gene expression in eukaryotes.

Results

Topoisomerase depletion impacts transcription dynamics genome-wide

To explore the genome-wide effect of DNA supercoiling on transcription, we perturbed supercoiling levels by acute degradation of the two main topoisomerases in *C. elegans*, TOP-1 and TOP-2, and profiled nascent transcription using GRO-seq. By coupling short topoisomerase depletion (1 hour) with the direct measurement of transcriptional output by GRO-seq, we aimed to detect the immediate and direct effects of supercoiling accumulation on transcription.

To study the individual contributions of TOP-1 and TOP-2 and their combined effect, we performed GRO-seq after depletion of either TOP-1 or TOP-2, and both. For this, we used our previously established worm strains containing the endogenous *top-1* and/or *top-2* genes tagged with *degron::GFP* and a transgene expressing the proteasome targeting protein TIR-1 in somatic tissues[27]. As controls, we used the degron::tagged strains that were not treated with auxin (no-auxin control) as well as a strain without a degron tag but containing the TIR-1 transgene that we treat with auxin (auxin control) (Figure 1A). After one hour auxin treatment of L2 larvae, we observe rapid disappearance of the GFP signal (Figure 1B).

In the control conditions, GRO-seq signal is distributed evenly along the gene body, with some genes showing a slight increase around transcription start site and most genes showing a prominent peak around the transcription end site (Figure 1C). The accumulation of the GRO-seq signal at the end of genes is consistent with previous reports suggesting slow 3' end processing in *C. elegans*[28,29] (Figure 1C, Supplementary Figure 1A).

Upon TOP-1 degradation, we observe a change in the distribution of GRO-seq signal, with some genes displaying an increase within the gene body and decrease across the transcription end site (Figure 1C upper panel, Supplementary Figure 1B). TOP-2 depletion alone did not result in detectable changes (Figure 1C, Supplementary Figure 1B). These results are consistent with previous reports indicating that TOP-1 has a non-redundant function in the resolution of transcription induced supercoiling[6,13,30].

When both topoisomerases were degraded, we observe a genome-wide alteration of the GRO-seq profile. In 83% of the expressed genes, the GRO-seq signal becomes concentrated

within the gene body and the TSS and TES peaks are lost (Figure 1C upper panel). RNA Pol II ChIP-seq performed in the same conditions also displayed increased gene body enrichment and reduced TSS and TES signal (Figure 1D upper panel). These results suggest that the absence of topoisomerases impacts the movement of transcribing RNA Pol II across genes, causing it to an accumulate within the gene body and reducing its 3' pausing.

In addition to the profile described above, 17% of the expressed genes show almost complete loss GRO-seq signal and RNA Pol II binding across the entire gene, suggesting reduced transcription initiation. Together, these results indicate that accumulation of DNA supercoiling impacts transcription dynamics genome-wide, influencing initiation, elongation and pausing of RNA Pol II.

TOP-1 and TOP-2 are required for elongation by RNA Polymerase II

Previous studies suggested that a defect in transcription elongation is more pronounced in longer genes that accumulate higher levels of supercoiling as RNA Pol II translocate across longer distances.[1] Indeed, longer genes showed a more drastic redistribution of nascent transcription (Figure 2A). In short genes, GRO-seq signal increases across the gene body but still shows a 3' bias, suggesting that a fraction of the RNA Pol II that initiated was able to reach the transcription end site (Figure 2A). This 3' bias gradually becomes less pronounced as the gene size increases, with the longest genes showing a 5' bias indicating that most of the transcribing RNA Pol II stop before reaching the end of the gene (Figure 2A and 2B).

Single TOP-1 degradation also led to stronger gene body accumulation of GRO-seq signal in longer genes (Supplementary Figure 2A), while no changes were observed upon TOP-2 degradation alone (Supplementary Figure 2B). Thus, our results indicate that TOP-1 is the major topoisomerase required for transcription elongation in *C. elegans*.

To understand the effect of transcription elongation on the RNA output, we investigated the relationship between the GRO-seq profiles and steady state RNA levels. We first profiled nuclear RNAs since they represent a more direct output of ongoing transcription. Depletion of TOP-1 and TOP-2 resulted in a relative increase and decrease in the RNA levels of genes shorter than 2 Kb and longer than 5 Kb, respectively (Figure 2C). These results are consistent with previous reports in yeast and mammals showing that the expression of long genes requires topoisomerase function[14,15].

In addition, nuclear RNA distribution along the gene mirrored the GRO-seq profile observed upon topoisomerase depletion, with long genes showing reduced transcript abundance towards the 3' end, whereas short genes are evenly covered (Figure 2B). This suggests that long transcripts remain unfinished whereas short transcripts are fully processed. To test this

interpretation, we sequenced total cellular RNAs and indeed found that the relative transcript level of longer genes is reduced upon topoisomerase depletion (Figure 2D). Compared to nuclear RNA-seq, we observe a stronger downregulation of long genes with total cellular RNA-seq, which might be due to degradation of long unfinished transcripts while short transcripts remain stable (Figure 2D). In summary, these results indicate that TOP-1/TOP-2 depletion results in transcription elongation problems that have a strong impact on long genes.

The effect of supercoiling on transcription of neighboring genes depends on their orientation

Next we explored the effect of topoisomerase depletion in the transcription of neighboring genes. The supercoiling status of a gene is influenced by its own transcription as well as transcription of the adjacent genes. Neighbors in a divergent orientation generate negative supercoiling between each other, whereas those in a convergent orientation produce positive supercoiling (Figure 3A). The supercoiling effect of tandemly oriented genes cancel each other (Figure 3A). Given that negative and positive supercoiling impact transcription-related processes in different ways[8,31], we hypothesized that accumulation of supercoiling upon topoisomerase depletion would have different outcomes for a gene depending on the orientation of its neighbors.

To investigate this, we classified genes based on the orientation of their two nearest neighbors into four groups (Figure 3C): 1) Tandem-Tandem: where both the gene behind and the gene ahead are in a tandem configuration (→→→, arrows represent gene orientation). 2) Divergent-Tandem: where one neighbor is divergent and the other is tandem (←→→). 3) Convergent-Tandem: where one neighbor is convergent and the other is tandem (→←←). 4) Divergent-Convergent: where one neighbor is divergent and the other is convergent (←→←).

First, we used differential gene expression analysis to identify genes showing strong changes in nascent transcription upon topoisomerase depletion. There were 2867 and 2968 genes with statistically significant (p value < 0.05) increase and decrease in the average GRO-seq signal, respectively (Figure 3B). These genes showed similar changes in RNA Pol II ChIP-seq and a subset of them was also affected in the single TOP-1 depletion condition (Supplementary Figure 3A, 3B and 3C). Next, we determined the proportion of Tandem-Tandem, Divergent-Tandem, Convergent-Tandem and Divergent-Convergent genes across the differentially expressed genes. We observe that the distribution of orientation groups is different between genes with increased and decreased GRO-seq (chi-square test p-value $<10^{-6}$) (Figure 3C).

Genes with increased GRO-seq signal upon TOP-1/TOP-2 depletion are enriched for genes with upstream and downstream neighbors transcribing away from the gene and therefore producing a negative supercoiling domain around the gene (Divergent-Tandem neighbors) (Figure 3C). The opposite is observed for genes with decreased GRO-seq signal, which are

enriched for those with upstream and downstream neighbors transcribing towards the gene and thus producing positive supercoiling in the direction of the gene (Convergent-Tandem neighbors) (Figure 3C). Genes with neighboring genes transcribed both away from and towards the gene (Divergent-Convergent and Tandem-Tandem) did not show a strong difference in GRO-seq signal upon TOP-1/TOP-2 depletion, suggesting that the effect of opposing supercoils may cancel each other. Analysis of transcription based on nuclear RNA-seq was consistent with results using GRO-seq (Figure 3D).

To test if the contrasting effect of TOP-1/TOP2 depletion on Divergent-Tandem and Convergent-Tandem genes is present genome-wide, we plotted GRO-seq log2 foldchanges for all the genes in each of the four groups shown in Figure 3A. Indeed, genes receiving negative supercoiling from neighboring genes showed increased levels of nascent transcription compared to those receiving positive supercoiling (Mann-Whitney test, two-tailed p-value $<10^{-15}$) (Figure 3E). Genes with neighbors transcribed both towards and away from are less affected. The same tendency was observed when data from nuclear RNA-seq was used (Figure 3F). Therefore, the effect of topoisomerase depletion is influenced by gene orientation, where divergent orientation promotes transcription while convergence has an inhibitory effect.

Divergent genes stimulate each other's transcription through negative supercoiling

We then asked if supercoiling could participate in coordinating expression of adjacent eukaryotic genes. Previous work in bacteria showed that negative supercoiling between divergent genes promotes transcription, while positive supercoiling generated by convergent orientation inhibits transcription[20,22–24]. Modelling studies have proposed similar effects in eukaryotes[17,18]. Here we sought *in vivo* evidence and a genome-wide view of how different types of supercoiling impact transcription of neighbor genes.

We hypothesized that if negative supercoiling has a stimulatory role in coordinating the expression of divergent genes, then increased expression of one gene should enhance the expression of its divergent neighbor and decreased expression should have an inhibitory effect. To investigate this, we plotted the correlation between log2 fold changes in GRO-seq for divergent, convergent and tandem gene pairs differentially expressed upon TOP-1/TOP-2 depletion. For this pairwise analysis, orientation was determined based on the closest neighbor. Upon topoisomerase depletion, changes in the expression of divergent gene pairs were positively correlated, while convergent gene pairs showed no correlation, and tandem genes showed a slight positive correlation (Figure 4A). Analyses using nuclear and total cellular RNA-seq data followed the tendency observed for GRO-seq (Figure 4B and Supplementary Figure 4A). Therefore, we conclude that when DNA supercoiling levels are perturbed, divergent and to lesser extent tandem genes pairs are affected synchronously while convergent genes have uncoordinated changes. This indicates that negative supercoiling enhances the expression of

neighbor genes and thus participate in their coordinated expression.

Positive supercoiling has been proposed to inhibit the transcription of convergent genes. In this case, higher transcription of a gene should result inhibit transcription of its convergent neighbor, resulting in a negative correlation. However, we observed no correlation between how the expression of convergent gene pairs change upon topoisomerase depletion (Figure 4A). Thus, we next asked to what extend neighboring genes expression correlate with each other. We plotted the correlation between the expression levels of gene pairs with different orientations separately in the control and TOP-1/TOP-2 depleted conditions. In the control, expression of neighbor genes for all the orientations showed a positive correlation (Figure 4C and Supplementary figure 4B) suggesting that in the presence of topoisomerases, convergent genes do not inhibit each other. In the absence of topoisomerases, the correlation between the expression of convergent genes is strongly affected, whereas the correlation between the expression of divergent genes is maintained (Figure 4C and Supplementary figure 4B). This suggests that an excess of positive supercoiling perturbs the coordinated expression of convergent genes while increased negative supercoiling between divergent genes does not disrupt their synchronized expression.

Impact of topoisomerases on histone modifications

During transcription, nucleosomes are disrupted ahead of RNA Pol II and reformed behind. Previous studies have shown that DNA torsion modulates nucleosome dynamics[6,32] but the impact of supercoiling on the distribution of histone modification remains unexplored. We decided to investigate if increased supercoiling in the absence of topoisomerases results in disruption of the histone modification landscape. Given the transcription elongation problem observed upon topoisomerases depletion, we profiled H3K36me3, which is deposited along gene bodies during transcription elongation. In addition, we profiled H3K27ac and H3K4me3, which are two active histone modifications enriched at enhancers and promoters, respectively, as well as the repressive mark H3K27me3.

Despite reduced transcriptional elongation, we do not observe significant changes in the profile of H3K36me3, even across long genes where the elongation defect is stronger (Figure 5A, Supplementary Figure 5A). On the other hand, we observe a slight decrease for H3K27ac and H3K4me3 around the transcription start site (Figure 5C and 5D). ChIP-seq analysis of TOP-1 and TOP-2[27] shows that both proteins bind to promoters and their binding correlates with H3K27Ac and H3K4me3 levels (Supplementary Figure 5B). Given that an interplay between histone modifiers and topoisomerases has been proposed[33,34], this effect on H3K27Ac and H3K4me3 could result from the absence of topoisomerases at promoters, or to the resulting supercoiling accumulation.

Discussion

In this study we combined independent methods to measure the effect of acute degradation of topoisomerases on ongoing transcription. This allowed us to interpret the complex impact of topoisomerase depletion on transcription initiation and elongation, and on the coupling of neighboring genes. We found that in *C. elegans*, topoisomerase I is required for transcription elongation and is partially redundant with topoisomerase II. Transcription elongation defects caused by TOP-1/TOP-2 depletion are stronger for long genes, where the transcribing polymerases do not reach the 3' end, resulting in reduced levels of processed transcripts. The effect of supercoiling on neighboring genes were dependent on the orientation of their transcription, indicating that negative supercoiling promotes coordinated and high transcription of divergent genes (Figure 6), while accumulation of excessive positive supercoiling disrupts coupling of convergent genes (Figure 6). Overall, our data indicates that DNA supercoiling produced by transcription at one point propagates along the chromatin fiber and influences transcription of neighboring genes in a manner dependent on their orientation.

Increased negative supercoiling promotes transcription

We observe that genes with upstream and downstream neighbors transcribing away from the gene (←→→, Divergent-Tandem genes) are induced upon TOP-1/TOP-2 depletion, while genes with upstream and downstream neighbors transcribing towards the gene (→←←, Convergent-Tandem) become repressed. In the context of gene triplets, genes surrounded by divergent and tandem neighbors receive negative supercoiling from both sides, whereas genes flanked by convergent and tandem neighbors only receive positive supercoiling. Therefore, these two groups of genes are under the influence of opposite supercoiling states that we propose drive their opposite response to topoisomerase depletion. In the case of genes with neighboring genes transcribed both away from and towards the gene (←→← Divergent-Convergent and →→→Tandem-Tandem), they receive both negative and positive supercoiling from their neighbors and show a milder response to topoisomerase degradation. We thus envision that for these genes, the effect of opposing supercoils may cancel each other. In summary our results are consistent with simulation studies predicting that negative supercoiling generated in the context of transcription of divergent genes acts to enhance their expression and positive supercoiling generated between convergent genes has an inhibitory effect[17,18,35]

The stimulatory effect of negative supercoiling accumulation was not observed in a recent study in yeast, where topoisomerase depletion led to inhibition of genes of all orientations[26]. Instead, it was proposed that the excess of both negative and positive supercoiling represses transcription by perturbing the binding of transcription factors. Negative supercoiling has been shown to promote binding of general transcription factors and other regulatory proteins[2–5,36]. Although we cannot exclude that excessive negative supercoiling resulting from the absence of topoisomerases could instead perturb protein binding to DNA, our results suggest that even in excess, negative supercoiling promotes neighboring transcription.

Coupling between convergent genes requires DNA supercoiling relaxation

Co-expression of adjacent genes is a strategy used by organisms to ensure coordinated expression of groups of genes sustaining transcriptional programs in response to the environment and during development[37]. Diffusion of DNA supercoiling could act as a rapid mechanism to regulate expression of genes in close proximity [17]. In the presence of topoisomerases, controlled levels of both positive and negative supercoiling might contribute to neighbors' co-expression, since the expression of gene pairs of all orientations is correlated in control conditions (Figure 4C)[38]. In the absence of topoisomerases, excessive levels of negative and positive supercoiling have different effects on co-expression of neighbor genes. While topoisomerase depletion did not affect correlated divergent genes, it perturbed coordinated expression of convergent genes. These results suggest that coordinated expression of neighbor genes requires tight regulation of positive supercoiling levels, whereas negative supercoiling levels are more flexible. Thus, we propose that the divergent orientation affords a more robust configuration for coordinated expression.

A non-catalytic role for topoisomerases in the regulation of histone modifications?

We hypothesized that DNA supercoiling could impact the deposition/removal of histone modifications by either its effect of transcription dynamics, which in turn would affect transcription-coupled histone modifications, or through its effect on nucleosome stability, which could impact how nucleosomes are displaced and reincorporated during transcription. We do not observe strong changes in the distribution of the elongation associated histone modification H3K36me3 upon topoisomerase depletion. This suggests that reduced transcription elongation in the absence of topoisomerases does not perturb the dynamics of H3K36me3. Moreover, although topoisomerase inactivation resulted in higher nucleosome turnover within the gene body[6], our data suggest that this does result in changes in the distribution of H3K36me3.

On the other hand, we observe a mild local reduction of H3K27ac and H3K4me3 around transcription start sites suggesting that DNA supercoiling could influence histone modifications associated with upstream regulatory elements. Another possibility is that this effect on H3K27ac and H3K4me3 is independent of the enzymatic activity of topoisomerases. A method developed to map catalytically engaged TOP-1 showed that it is depleted at promoters and becomes enriched within the gene body[39]. Yet, chromatin immunoprecipitation experiments of TOP-1 and TOP-2 in various organisms showed their accumulation at promoters[27,30,39,40]. Therefore, binding at promoters is evolutionarily conserved but might not reflect catalytically engaged forms of topoisomerases. Instead, promoter associated topoisomerases might function through a non-catalytic mechanism, regulating transcription and chromatin structure through protein-protein interactions.

In summary, our study provides evidence for a role of DNA supercoiling in coupling transcription between neighbor genes, highlighting the impact of DNA structure and topoisomerases as key transcriptional regulators.

Acknowledgments

G.C., A.C. and A.K.M. have received funding from the Institut Pasteur, the CNRS, and the European Research Council (ERC) under the European Union's Horizon 2020 research and innovation program under grant agreement number 101002999. A.K.M. was also supported by a LabEx Revive fellowship ANR-10-LBX-73. S.E., Y.Z., and A.K.M and research in this article were supported by NIGMS of the National Institutes of Health under award number R35 GM130311.

Author contributions

A.K.M, G.C. and S.E. conceptualized the project and designed experiments. A.K.M. and Y.Z. performed experiments. A.K.M. and A.C. performed bioinformatics analysis. A.K.M. wrote the manuscript with input from S.E. and G.C.

Declaration of interests:

The authors declare no competing interest.

Materials and methods

Worm strains and growth

Worms were grown and maintained at 20°C on Nematode Growth Medium (NGM) plates containing the *E. coli* strain OP50. To isolate synchronized L2 worms, gravid adults were bleached in 0.5 M NaOH and 1.2% bleach, and embryos were hatched overnight in M9 buffer (22 mM KH2PO4 monobasic, 42.3 m in M Na2HPO4, 85.6 mM NaCl, 1mM MgSO4). Starved L1s were grown for 24 hours at 22°C in plates seeded with OP50 and the resulting L2 worms were used for auxin treatment. The *top-1::degron::GFP* and *top-2::degron::GFP* worms strains used in this study were previously described in Morao, *et al* 2022[27]

Auxin treatment

A 400 mM auxin (indole-3-acetic-acid, Fisher 87-51-4) solution was prepared by resuspending auxin powder in 100% ethanol. 1 mM auxin plates were prepared by adding resuspended auxin to NGM media before pouring the plates. Around 10^5 synchronized L2 worms obtained as

described above were washed three times with M9 and divided in two aliquots. Half of the worms was transferred to NGM 15 cm plates supplemented with 1 mM of auxin. The other half was transferred to normal NGM 15 cm plates. Both auxin and no-auxin conditions were incubated for one hour at room temperature. Worms were then washed once with M9 and stored accordingly to future application. For GRO-seq and Cut & Tag, worms were stored in M9 buffer at -20 C till further processing. For RNA-seq, worms were stored in Trizol. For ChIP, worms were crosslinked in 2% formaldehyde for 30 minutes, followed by quenching in 125 mM glycine for 5 minutes, one wash with M9 and two washes with PBS, PMSF and protease inhibitors.

Nuclei preparation for GRO-seq and Cut&Tag

Worms were resuspended in 2 mL of nuclei extraction buffer (20 mM HEPES–KOH, pH 7.9, 10 mM KCl, 0.1% Triton X-100, 20% Glycerol, 0.5 mM spermidine, protease inhibitors) and lysed by applying 100 strokes with a stainless-steel tissue grinder. Lysates were centrifuged at 100 g for 4 minutes at 4C to remove debris. Supernatants were transferred to 1.5 mL low binding microcentrifuge tubes and nuclei were pelleted by centrifuging at 1000 g for 4 minutes at 4C. Nuclei were washed 3 times with nuclei extraction buffer by repeated centrifugation at 1000 g for 4 minutes at 4C and resuspension in 1 mL of nuclei extraction buffer. For GRO-seq, nuclei were resuspended in 100 µL of freezing buffer (50 mM Tris-HCl pH 8, 5 mM $MgCl_2$, 0.1 mM EDTA). For Cut&Tag, nuclei were resuspended in 500 µL of nuclei extraction buffer.

GRO-seq

GRO-seq was performed as previously described[41]. Briefly, nuclear Run-On reactions were performed by incorporating 1 mM Bio-11UTP, followed by RNA extraction with Trizol and RNA fragmentation. Biotinylated nascent RNA was then purified using Dynabead™ MyOne™ Streptavidin C1 (Cat#65001). To prepare libraries, purified RNAs were first treated with T4 Polynucleotide Kinase (New England Biolabs) to repair the 5'-OH ends. This was followed by 3' and 5' adaptor ligation. Adaptor-ligated RNAs were then reverse transcribed using SuperScript IV Reverse Transcriptase (Thermo Fisher Scientific), following the manufacturer's protocol with slight modifications: the reaction was incubated for 1 hour at 50°C and 10 minutes at 80°C. cDNA was PCR amplified using specific primers and the NEBNext Ultra II Q5 Master Mix 2x (New England Biolabs) for 15 cycles. Libraries were analyzed using the Agilent 2200 TapeStation System with high sensitivity D1000 screentapes and quantified with the Qubit Fluorometer High Sensitivity dsDNA assay kit (Thermo Fisher Scientific, Q32851). The multiplexed libraries were then sequenced on the Illumina NextSeq 2000 platform. Analysis of the sequencing data was performed as described in Quarato, et al 2021[41]. The scripts and workflows are available at https://gitlab.pasteur.fr/bli/bioinfo_utils. Two biological replicates were performed for each experiment.

Cut&Tag

Cut&Tag was performed following the EpiCypher protocol with few modifications. Briefly, 100 µL of the nuclei resuspension generated as described above were used for binding to Convanavalin A beads (Epicypher 21-1401). Bead-bound nuclei were resuspended in 100 µL of Antibody150 buffer (20 mM HEPES pH 7.5, 150 mM NaCl, 0.01% digitonin, 2 mM EDTA, protease inhibitors, 0.5 mM spermidine) and 1 µg of primary antibody was added. Reactions were incubated overnight in a thermocycler shaker set up at 4 C with shaking cycles at 2000 rpm 15 seconds ON 45 seconds OFF. 1 µg of secondary antibody was added followed by tagmentation with Tn5 (Epicypher 15-1117). Resulting libraries were amplified with i5 and i7 primers using 13 PCR cycles and purified using AMPure beads. Libraries were analyzed using the Agilent 2200 TapeStation System with high sensitivity D1000 screentapes and quantified with the Qubit Fluorometer High Sensitivity dsDNA assay kit (Thermo Fisher Scientific, Q32851). Three biological replicates were performed for each experiment.

Cut&Tag data processing and analysis

Reads were aligned with Bowtie2[42] to the WBcel235 genome, with the following options: "--local --very-sensitive-local --dovetail --soft-clipped-unmapped-tlen". Reads were additionally deduplicated using samtools and filtered to keep those with a single discovered alignment. Peaks were called using MACS2 with the following parameters: "callpeak -q 0.05 -g ce --keep-dup all". Peaks were further filtered to keep those with MACS2 FDR < 0.01 in merged reads from all conditions, and FDR < 0.05 in at least two individual replicates. Quantifications for the selected set of the peaks were done for each dataset using Subread featureCounts and analyzed using a DESeq2 generalized linear model.

RNA-seq

Total RNA was purified following Trizol manufacturer's instructions after freeze-cracking samples five times. DNase treatment was performed using 2 µg of total RNA by treating with 2 U Turbo DNase (Ambion) at 37 C for 30 min followed by acid phenol extraction and ethanol precipitation. The Agilent 2200 TapeStation System was used to calculate the RIN indexes of RNA samples, and only samples with RIN > 8 were used for library preparation. For strand-specific RNA-seq library preparation, DNase-treated total RNA was used for ribosomal and mitochondrial rRNAs depletion following a custom RNAse-H-based method to degrade rRNAs based on complementary oligos, as described in Barucci et al., 2020[43]. Strand-specific RNA libraries were prepared using around 1µg of rRNA depleted RNAs with the NEBNext Ultra II Directional RNA Library Prep Kit for Illumina (E7760S). The size distribution of the RNA libraries was determined with Agilent 2200 TapeStation System using high sensitivity D1000 screentapes. Libraries were

quantified using the Qubit Fluorometer High Sensitivity dsDNA assay kit (Thermo Fisher Scientific, Q32851). Two biological replicates were performed for each experiment.

RNA-seq data processing and analysis

RNA-seq reads were aligned to the WBcel235 genome using STAR[44] and quantified by RSEM[45] using the RSEM-STAR pipeline with the following additional options: '--calc-pme --calc-ci --estimate-rspd'. Further analysis was conducted using the Bioconductor DESeq2 package[46] from gene-level values for rounded RSEM counts. Genes with at least 10 normalized counts in all replicates were considered for differential expression analysis. Differential expression between replicate groups was assessed using Wald Test, thresholding for significance at: FDR <= 0.05. Principal Component Analysis (PCA) and data visualization were made in R using 'prcomp' function and ggplot2 package[47].

ChIP-seq

Approximately 100 µL of pelleted L2 larvae were resuspended in FA buffer (150 mM NaCl, 50 mM HEPES/KOH pH 7.5, 1 mM EDTA, 1% Triton X-100, 0.1% sodium deoxycholate), supplemented with PMSF and protease inhibitors (Calbiochem, 539131), and lysed with 30 strokes of a glass homogenizer (Douncer). The lysates were sonicated for 15 minutes in 0.1% sarkosyl using a Bioruptor-pico. Protein concentration was measured using the Bradford assay (Biorad 500-0006), and 2 mg of protein extract were used for each ChIP (volume: 460 µL). A 5% aliquot was reserved as input DNA. The remaining protein extract was incubated with 5 µg of 8WG16 antibody (Millipore 05-952-I) at 4°C overnight with rotation. Next, 20 µL of Protein A and G Sepharose beads were washed three times with FA buffer and added to the immunoprecipitation reaction, which was rotated at 4°C for 2 hours. The beads were then washed with 1 mL of each of the following buffers: twice with FA buffer, once with FA-1 mM NaCl, once with FA-500 mM NaCl, once with TEL buffer (0.25 M LiCl, 1% NP-40, 1% sodium deoxycholate, 1 mM EDTA, 10 mM Tris-HCl pH 8.0), and twice with TE buffer. Immunoprecipitated DNA was eluted from the beads by incubating with ChIP elution buffer (1% SDS, 250 mM NaCl, 10 mM Tris pH 8.0, 1 mM EDTA) at 65°C for 30 minutes and then reverse-crosslinked at 65°C overnight in a water bath. For library preparation, half of the ChIP DNA and 30 ng of input DNA were ligated to Illumina TruSeq adapters and amplified by PCR. DNA fragments between 250 and 600 bp were gel-purified using the Qiagen gel extraction kit. Sequencing was performed using single-end 75 bp reads on the Illumina NextSeq 500 at the New York University Center for Genomics and Systems Biology. Two biological replicates with matching input samples were performed for each experiment.

ChIP-seq data processing and analysis

Bowtie2 version 2.4.2 was used to align 75 bp single-end reads to the WS220 reference genome using default parameters[42]. BAM file sorting and indexing were performed with Samtools version

1.11[48]. BamCompare tool in Deeptools version 3.5.0 was used to normalize for the sequencing depth using CPM and create ChIP-Input coverage and ChIP/Input ratios with a bin size of 10 bp and 200 bp read extension[49]. Only reads with a minimum mapping quality of 20 were included, and mitochondrial DNA, PCR duplicates, and blacklisted genomic regions were excluded[50]. To generate average coverage data, ChIP-Input enrichment scores were averaged across 10 bp bins throughout the genome.

References

1. Liu, L. F. & Wang, J. C. Supercoiling of the DNA template during transcription. *Proc. Natl. Acad. Sci.* **84**, 7024–7027 (1987).
2. Kouzine, F., Liu, J., Sanford, S., Chung, H.-J. & Levens, D. The dynamic response of upstream DNA to transcription-generated torsional stress. *Nat. Struct. Mol. Biol.* **11**, 1092–1100 (2004).
3. Kouzine, F., Sanford, S., Elisha-Feil, Z. & Levens, D. The functional response of upstream DNA to dynamic supercoiling in vivo. *Nat. Struct. Mol. Biol.* **15**, 146–154 (2008).
4. Mizutani, M., Ohta, T., Watanabe, H., Handa, H. & Hirose, S. Negative supercoiling of DNA facilitates an interaction between transcription factor IID and the fibroin gene promoter. *Proc. Natl. Acad. Sci.* **88**, 718–722 (1991).
5. Parvin, J. D. & Sharp, P. A. DNA topology and a minimal set of basal factors for transcription by RNA polymerase II. *Cell* **73**, 533–540 (1993).
6. Teves, S. S. & Henikoff, S. Transcription-generated torsional stress destabilizes nucleosomes. *Nat. Struct. Mol. Biol.* **21**, 88–94 (2014).
7. Sheinin, M. Y., Li, M., Soltani, M., Luger, K. & Wang, M. D. Torque modulates nucleosome stability and facilitates H2A/H2B dimer loss. *Nat. Commun.* **4**, 2579 (2013).
8. Ma, J. & Wang, M. D. DNA supercoiling during transcription. *Biophys. Rev.* **8**, 75–87 (2016).
9. Pedersen, J. M. *et al.* DNA Topoisomerases Maintain Promoters in a State Competent for Transcriptional Activation in Saccharomyces cerevisiae. *PLOS Genet.* **8**, e1003128 (2012).
10. Chong, S., Chen, C., Ge, H. & Xie, X. S. Mechanism of Transcriptional Bursting in Bacteria. *Cell* **158**, 314–326 (2014).
11. Baranello, L., Kouzine, F. & Levens, D. DNA Topoisomerases. *Transcription* **4**, 232–237 (2013).
12. Pommier, Y., Sun, Y., Huang, S. N. & Nitiss, J. L. Roles of eukaryotic topoisomerases in transcription, replication and genomic stability. *Nat. Rev. Mol. Cell Biol.* **17**, 703–721 (2016).
13. Sperling, A. S., Jeong, K. S., Kitada, T. & Grunstein, M. Topoisomerase II binds nucleosome-free DNA and acts redundantly with topoisomerase I to enhance recruitment of RNA Pol II in budding yeast. *Proc. Natl. Acad. Sci. U. S. A.* **108**, 12693–12698 (2011).
14. King, I. F. *et al.* Topoisomerases facilitate transcription of long genes linked to autism. *Nature* **501**, 58–62 (2013).

15. Joshi, R. S., Piña, B. & Roca, J. Topoisomerase II is required for the production of long Pol II gene transcripts in yeast. *Nucleic Acids Res.* **40**, 7907–7915 (2012).
16. Kouzine, F. *et al.* Transcription-dependent dynamic supercoiling is a short-range genomic force. *Nat. Struct. Mol. Biol.* **20**, 396–403 (2013).
17. Johnstone, C. P. & Galloway, K. E. Supercoiling-mediated feedback rapidly couples and tunes transcription. *Cell Rep.* **41**, 111492 (2022).
18. Ancona, M., Bentivoglio, A., Brackley, C. A., Gonnella, G. & Marenduzzo, D. Transcriptional Bursts in a Nonequilibrium Model for Gene Regulation by Supercoiling. *Biophys. J.* **117**, 369–376 (2019).
19. El Houdaigui, B. *et al.* Bacterial genome architecture shapes global transcriptional regulation by DNA supercoiling. *Nucleic Acids Res.* **47**, 5648–5657 (2019).
20. Sobetzko, P. Transcription-coupled DNA supercoiling dictates the chromosomal arrangement of bacterial genes. *Nucleic Acids Res.* **44**, 1514–1524 (2016).
21. Meyer, S. & Beslon, G. Torsion-Mediated Interaction between Adjacent Genes. *PLOS Comput. Biol.* **10**, e1003785 (2014).
22. Hanafi, D. E. & Bossi, L. Activation and silencing of leu-500 promoter by transcription-induced DNA supercoiling in the Salmonella chromosome. *Mol. Microbiol.* **37**, 583–594 (2000).
23. Rhee, K. Y. *et al.* Transcriptional coupling between the divergent promoters of a prototypic LysR-type regulatory system, the ilvYC operon of Escherichia coli. *Proc. Natl. Acad. Sci.* **96**, 14294–14299 (1999).
24. Chen, C.-C., Chou, M.-Y., Huang, C.-H., Majumder, A. & Wu, H.-Y. A Cis-spreading Nucleoprotein Filament Is Responsible for the Gene Silencing Activity Found in the Promoter Relay Mechanism *. *J. Biol. Chem.* **280**, 5101–5112 (2005).
25. Bancaud, A. *et al.* Structural plasticity of single chromatin fibers revealed by torsional manipulation. *Nat. Struct. Mol. Biol.* **13**, 444–450 (2006).
26. Patel, H. P. *et al.* DNA supercoiling restricts the transcriptional bursting of neighboring eukaryotic genes.
27. Morao, A. K., Kim, J., Obaji, D., Sun, S. & Ercan, S. Topoisomerases I and II facilitate condensin DC translocation to organize and repress X chromosomes in C. elegans. *Mol. Cell* **82**, 4202-4217.e5 (2022).
28. Kruesi, W. S., Core, L. J., Waters, C. T., Lis, J. T. & Meyer, B. J. Condensin controls recruitment of RNA polymerase II to achieve nematode X-chromosome dosage compensation. *eLife* **2**, e00808 (2013).
29. Cecere, G., Hoersch, S., Jensen, M. B., Dixit, S. & Grishok, A. The ZFP-1(AF10)/DOT-1 Complex Opposes H2B Ubiquitination to Reduce Pol II Transcription. *Mol. Cell* **50**, 894–907 (2013).
30. Durand-Dubief, M., Persson, J., Norman, U., Hartsuiker, E. & Ekwall, K. Topoisomerase I regulates open chromatin and controls gene expression in vivo. *EMBO J.* **29**, 2126–2134 (2010).
31. Corless, S. & Gilbert, N. Effects of DNA supercoiling on chromatin architecture. *Biophys. Rev.* **8**, 245–258 (2016).

32. Achar, Y. J., Adhil, M., Choudhary, R., Gilbert, N. & Foiani, M. Negative supercoil at gene boundaries modulates gene topology. *Nature* **577**, 701–705 (2020).
33. Husain, A. *et al.* Chromatin remodeller SMARCA4 recruits topoisomerase 1 and suppresses transcription-associated genomic instability. *Nat. Commun.* **7**, 10549 (2016).
34. Dykhuizen, E. C. *et al.* BAF complexes facilitate decatenation of DNA by topoisomerase IIα. *Nature* **497**, 624–627 (2013).
35. Brackley, C. A. *et al.* Stochastic Model of Supercoiling-Dependent Transcription. *Phys. Rev. Lett.* **117**, 018101 (2016).
36. Tabuchi, H., Handa, H. & Hirose, S. Underwinding of DNA on Binding of Yeast TFIID to the TATA Element. *Biochem. Biophys. Res. Commun.* **192**, 1432–1438 (1993).
37. Zinani, O. Q. H., Keseroğlu, K. & Özbudak, E. M. Regulatory mechanisms ensuring coordinated expression of functionally related genes. *Trends Genet.* **38**, 73–81 (2022).
38. Cohen, B. A., Mitra, R. D., Hughes, J. D. & Church, G. M. A computational analysis of whole-genome expression data reveals chromosomal domains of gene expression. *Nat. Genet.* **26**, 183–186 (2000).
39. Baranello, L. *et al.* RNA Polymerase II Regulates Topoisomerase 1 Activity to Favor Efficient Transcription. *Cell* **165**, 357–371 (2016).
40. Ahmed, W. *et al.* Transcription facilitated genome-wide recruitment of topoisomerase I and DNA gyrase. *PLOS Genet.* **13**, e1006754 (2017).
41. Quarato, P. & Cecere, G. Global Run-On sequencing to measure nascent transcription in C. elegans. *STAR Protoc.* **2**, 100991 (2021).
42. Langmead, B. & Salzberg, S. L. Fast gapped-read alignment with Bowtie 2. *Nat. Methods* **9**, 357–359 (2012).
43. Barucci, G. *et al.* Small-RNA-mediated transgenerational silencing of histone genes impairs fertility in piRNA mutants. *Nat. Cell Biol.* **22**, 235–245 (2020).
44. Dobin, A. *et al.* STAR: ultrafast universal RNA-seq aligner. *Bioinformatics* **29**, 15–21 (2013).
45. Li, B. & Dewey, C. N. RSEM: accurate transcript quantification from RNA-Seq data with or without a reference genome. *BMC Bioinformatics* **12**, 1–16 (2011).
46. Love, M. I., Huber, W. & Anders, S. Moderated estimation of fold change and dispersion for RNA-seq data with DESeq2. *Genome Biol.* **15**, 550 (2014).
47. Wickham, H. *Ggplot2*. (Springer International Publishing, Cham, 2016). doi:10.1007/978-3-319-24277-4.
48. Danecek, P. *et al.* Twelve years of SAMtools and BCFtools. *GigaScience* **10**, giab008 (2021).
49. Ramírez, F. *et al.* deepTools2: a next generation web server for deep-sequencing data analysis. *Nucleic Acids Res.* **44**, W160-165 (2016).
50. Amemiya, H. M., Kundaje, A. & Boyle, A. P. The ENCODE Blacklist: Identification of Problematic Regions of the Genome. *Sci. Rep.* **9**, 9354 (2019).

Figure 1

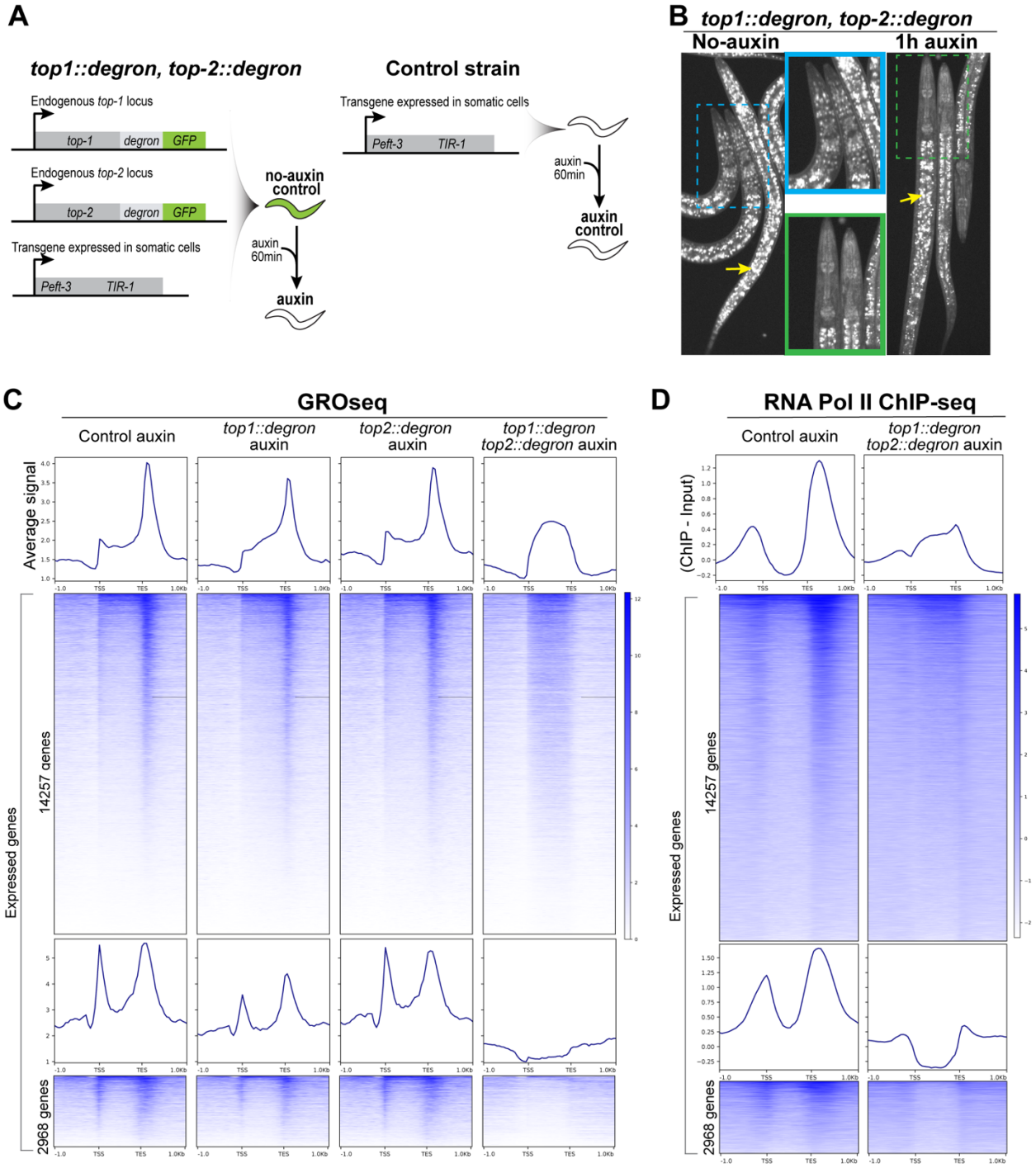

Figure 1. Topoisomerase depletion impacts transcription dynamics genome-wide

A Schematic representation of the worm strains used for the auxin-inducible degradation of TOP-1 and TOP-2. As controls, we used degron-tagged worms that were not treated with auxin (no-auxin control), and a strain without the degron tag but containing the TIR-1 transgene, that was treated with auxin (auxin control).

B Images of *top-1::degron::GFP, top-2::degron::GFP* worms incubated for one hour in plates containing auxin. Yellow arrows indicate autofluorescent gut granules present throughout the intestine.

C Heatmaps showing GRO-seq signal across expressed genes in control, *top-1::degron, top-2::degron and top-1::degron,top-2::degron* auxin conditions. Genes were grouped based on their GRO-seq profile upon TOP-1/TOP-2 depletion in two groups: 1. Top panel: genes where GRO-seq signal is decreased around the TSS and the TES and accumulates within the gene body. 2. Bottom panel: genes with overall reduced GRO-seq signal. Average plots are included at the top of the heatmaps.

D Heatmap showing RNA Pol-II ChIP-seq signal across expressed genes in control *and top-1::degron,top-2::degron* auxin conditions. Similar to **C**, genes were grouped based on their GRO-seq profile upon TOP-1/TOP-2 depletion in two groups. Average plots are included at the top.

Figure 2

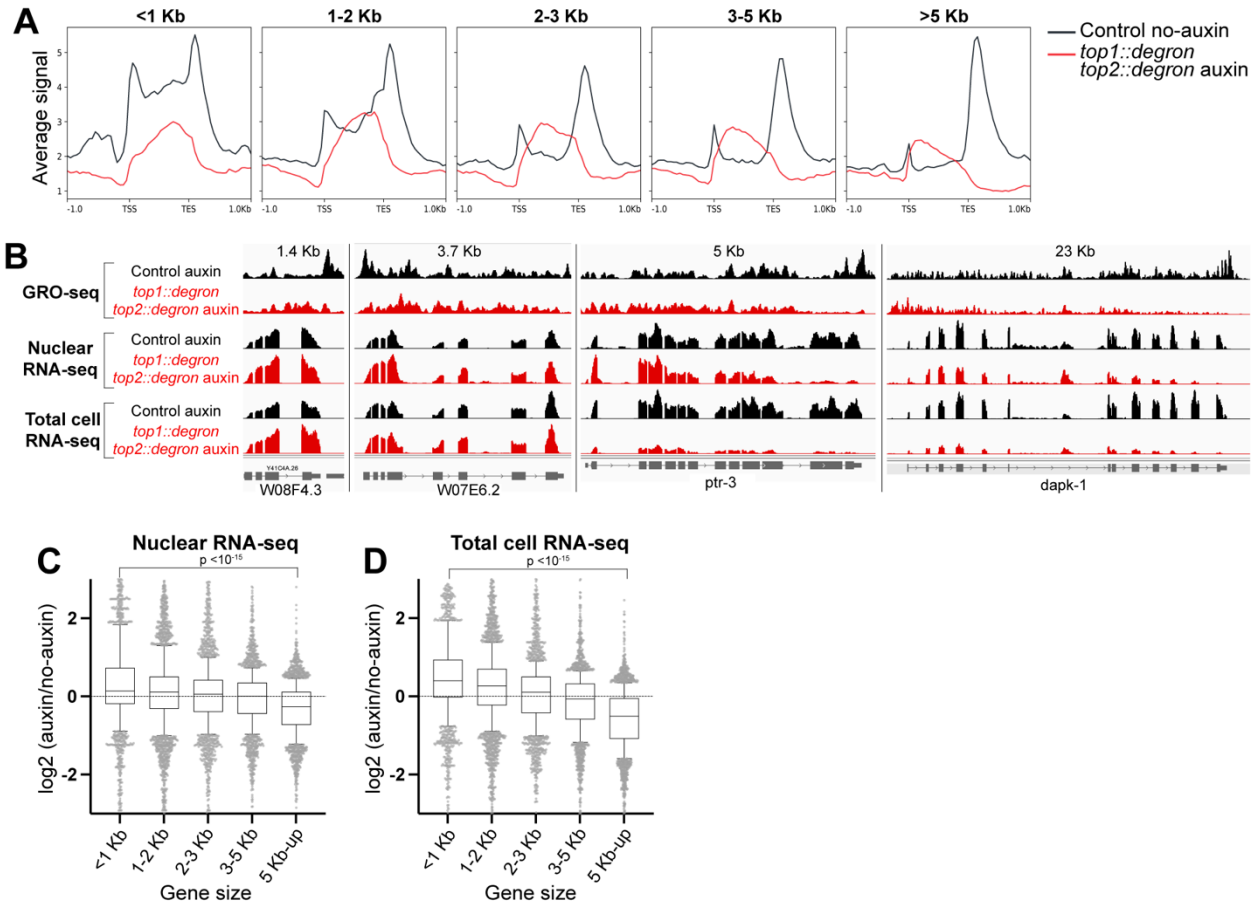

Figure 2. TOP-1 and TOP-2 are required for elongation by RNA Polymerase II

A Average GRO-seq scores in control (black) and TOP-1/TOP-2 depletion (red) are plotted across genes grouped based on their length into five categories: < 1 Kb, 1-2 Kb, 2-3 Kb, 3-5 Kb and > 5 Kb.

B IGV screenshots of GRO-seq, nuclear RNA-seq and total cellular RNA-seq profiles in control and TOP-1/TOP-2 depleted conditions at representative genes of different sizes. The size of the genes is indicated at the top. In the absence of topoisomerases, long genes show a progressive decrease of nuclear RNA levels towards the TES.

C Nuclear RNA-seq log2 fold changes between the auxin and no-auxin conditions are shown for genes of different sizes. Boxplots display median (line), first, and third quartiles (box), and 90th/10th percentile values (whiskers). For comparison between shortest (< 1Kb) and longest genes (> 5 Kb), two-tailed p-values were calculated using Mann-Whitney-Wilcoxon tests.

D Total cell RNA-seq log2 fold changes between the auxin and no-auxin conditions are shown for genes of different sizes. For comparison between shortest (< 1Kb) and longest genes (> 5 Kb), two-tailed p-values were calculated using Mann-Whitney-Wilcoxon tests.

Figure 3

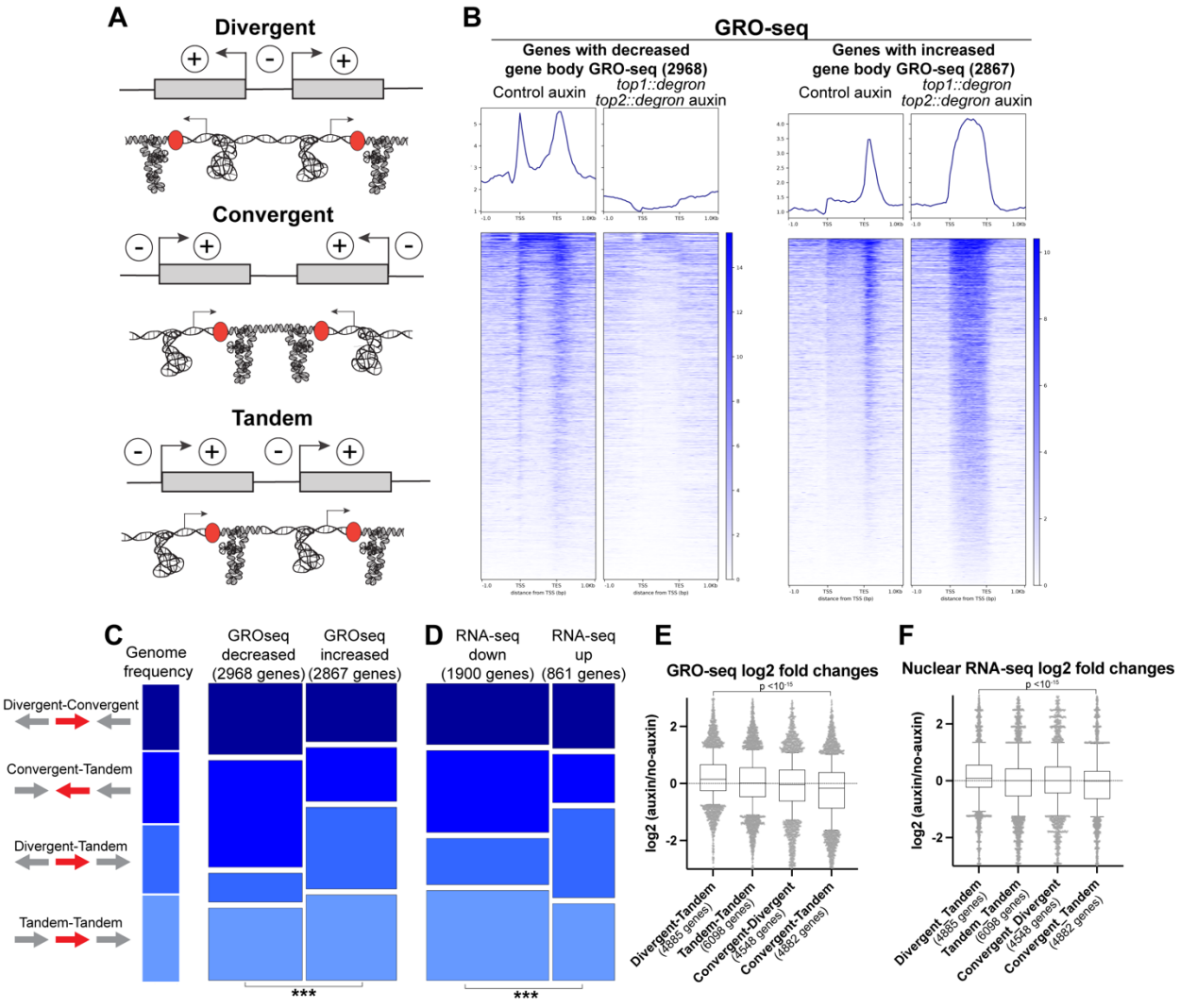

Figure 3. The effect of supercoiling on transcription of neighboring genes depends on their orientation

A Schematic representation of gene pairs with different orientations. Negative and positive supercoiling generated by their transcription is indicated by (-) and (+) and represented by under and over-wounded DNA.

B Heatmap showing GRO-seq scores for control auxin and *top-1::degron,top-2::degron* auxin . Genes with significant (pvalue < 0.05) decreased gene body GRO-seq are on the left and genes with increased gene body GRO-seq are on the right.

C Genes were classified based of the orientation of their upstream and downstream neighbors into four groups colored in different tonalities of blue: Divergent-Convergent, Convergent-Tandem, Divergent-Tandem and Tandem-Tandem. The height of the of the bars represents the proportion of genes belonging to each orientation group. This proportion is shown for the genome (left) and for genes with increased and decreased GRO-seq signal (right). Asterisks at the bottom indicate

significance of the difference between genes with decreased and increased GRO-seq (chi-square test p-value $<10^{-6}$).

D Distribution of orientation groups across genes found down and regulated by nuclear RNA-seq is represented as in **C**.

E GRO-seq log2 fold changes between the auxin and no-auxin conditions are shown for Divergent-Tandem, Tandem-Tandem, Divergent-Convergent and Convergent-Tandem genes. Boxplots display median (line), first, and third quartiles (box), and 90th/10th percentile values (whiskers). For comparison between Divergent-Tandem and Convergent-Tandem genes, two-tailed p-values were calculated using Mann-Whitney-Wilcoxon tests. The number of genes in each group is shown in parenthesis.

F Nuclear RNA-seq log2 fold changes between the auxin and no-auxin conditions are shown for Divergent-Tandem, Tandem-Tandem, Divergent-Convergent and Convergent-Tandem genes. Boxplots display median (line), first, and third quartiles (box), and 90th/10th percentile values (whiskers). For comparison between Divergent-Tandem and Convergent-Tandem genes, two-tailed p-values were calculated using Mann-Whitney-Wilcoxon tests. The number of genes in each group is shown in parenthesis.

Figure 4

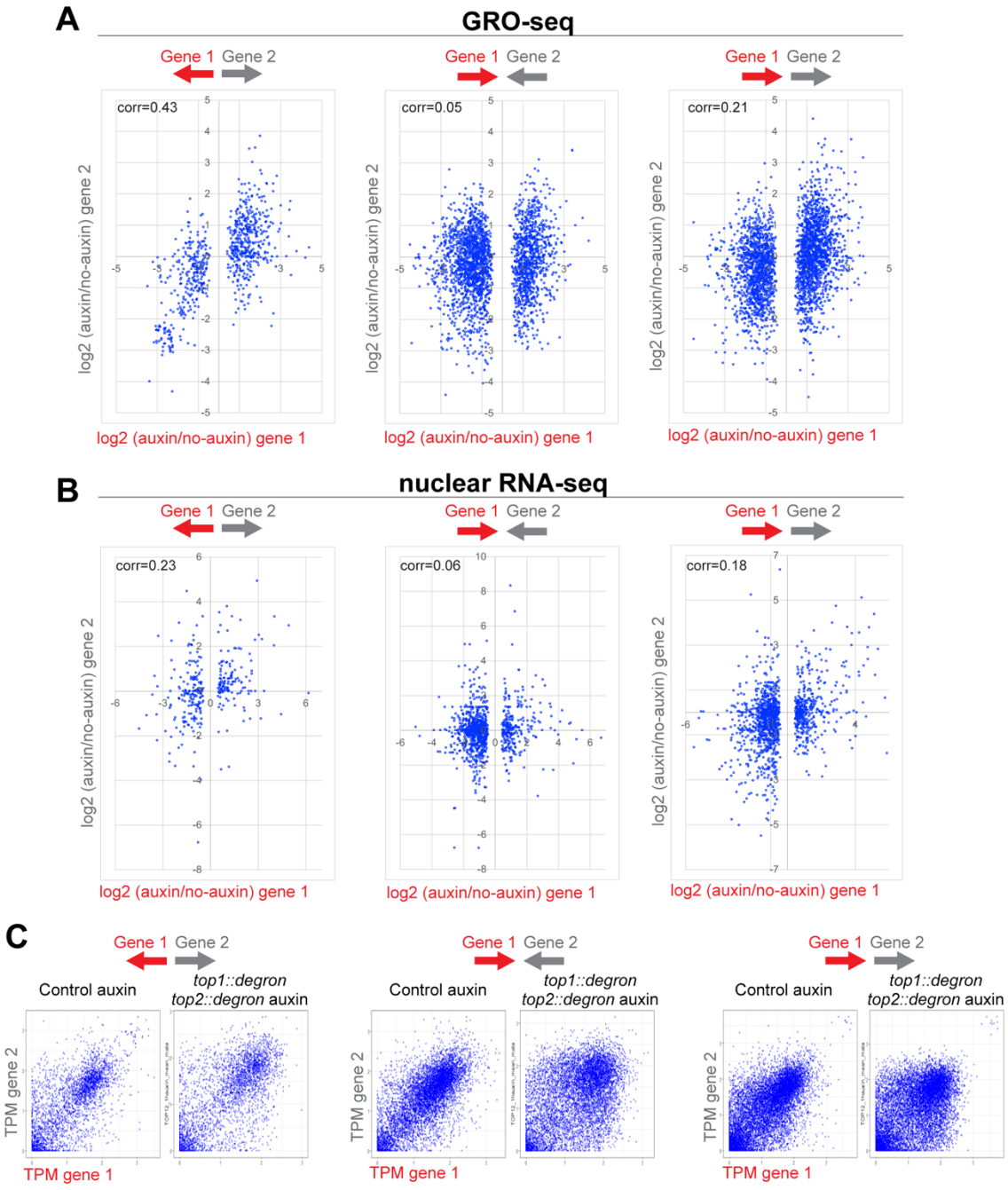

Figure 4. Divergent genes stimulate each other's transcription through negative supercoiling

A Scatter plot showing GRO-seq log2-fold changes between the *top-1::degron,top-2::degron* auxin and no-auxin conditions for gene pairs with different orientations.

B Scatter plot showing nuclear RNA-seq log2-fold changes between the *top-1::degron,top-2::degron* auxin and no-auxin samples for gene pairs with different orientations.

C Scatter plot showing GRO-seq TPM values in control and *top-1::degron,top-2::degron* auxin for gene pairs with different orientations.

Figure 5

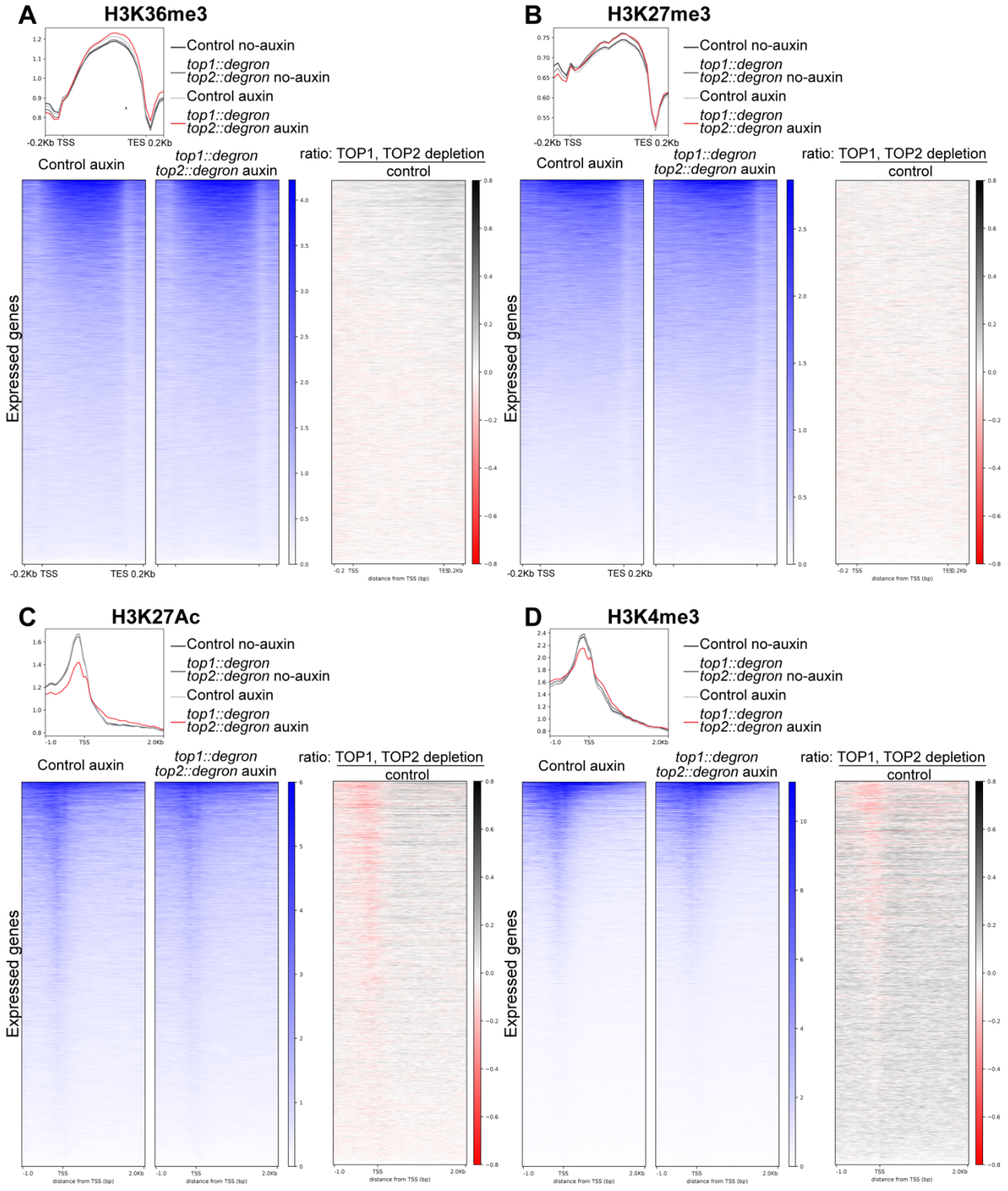

Figure 5. Impact of topoisomerases on histone modifications

A,B,C,D Heatmap showing H3K36me3 **(A)**, H3K27me3 **(B)**, H3K27ac **(C)** and H3K4me3 **(D)** Cut & Tag signal across expressed genes in control *and top-1::degron, top-2::degron* auxin conditions. Average plots including the no-auxin and auxin controls are included at the top. Heatmaps of the ratios between the TOP-1/TOP-2 depleted condition and the control are included on the right. For H3K27Ac and H3K4me3, signal around the TSS is shown. For H3K36 and H3K27me3, gene bodies were scaled to 1Kb.

Figure 6

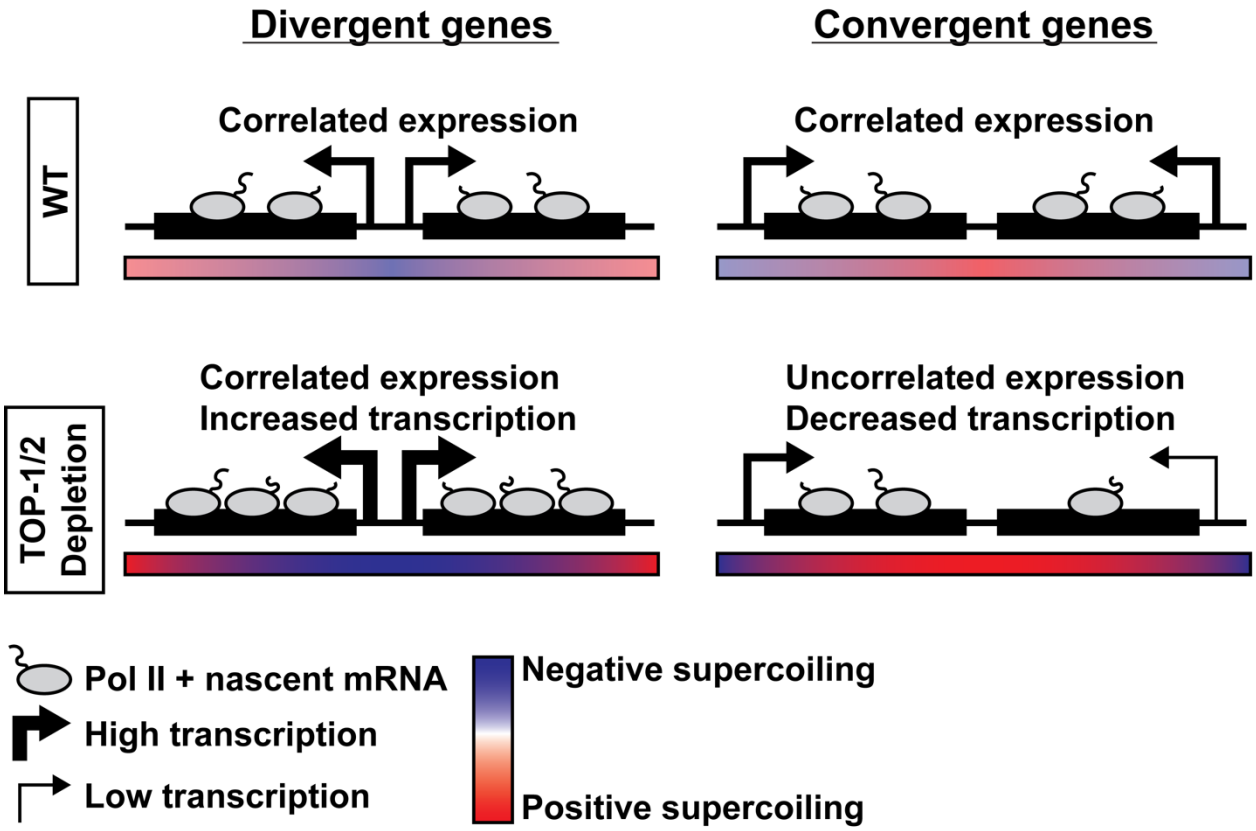

Figure 6

Model for the effect of topoisomerase depletion on the transcription of divergent and convergent genes.

Supplementary Figure 1

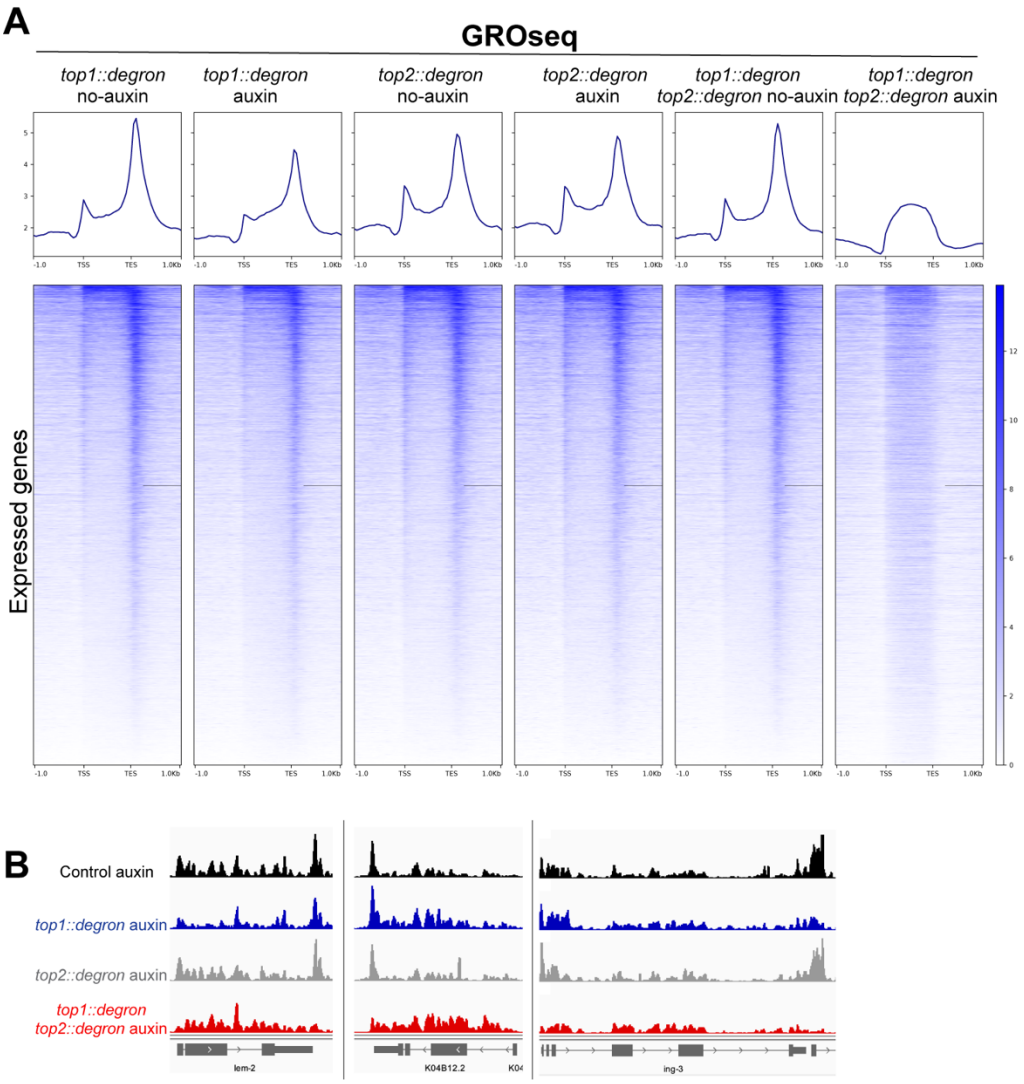

Supplementary Figure 1

A Heatmap showing GRO-seq signal across expressed genes in *top-1::degron, top-2::degron and top-1::degron, top-2::degron* no-auxin and auxin conditions. Average plots are included at the top. **B** IGV screenshots of GRO-seq scores in control, TOP-1, TOP-2 and TOP-1/TOP-2 depleted conditions at genes showing no changes (left), increased gene body signal (middle) and reduced TES peak (right) in the TOP-1 depletion.

Supplementary Figure 2

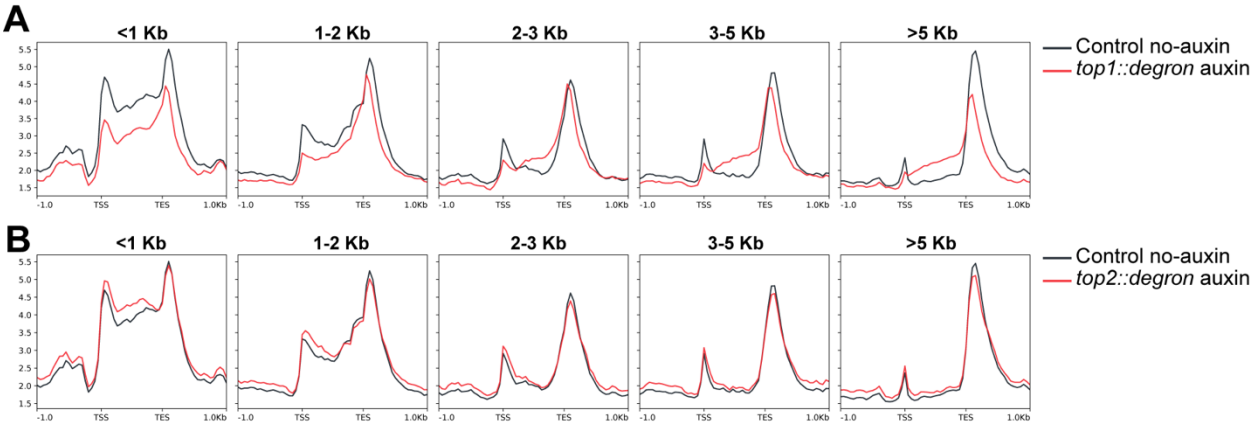

Supplementary Figure 2

A Average GRO-seq scores in control (black) and TOP-1 depletion (red) are plotted across genes grouped based on their length into five categories: <1 Kb, 1-2 Kb, 2-3 Kb, 3-5 Kb and >5 Kb.

B Average GRO-seq scores in control (black) and TOP-2 depletion (red) are plotted across genes grouped based on their length into five categories: <1 Kb, 1-2 Kb, 2-3 Kb, 3-5 Kb and >5 Kb.

Supplementary Figure 3

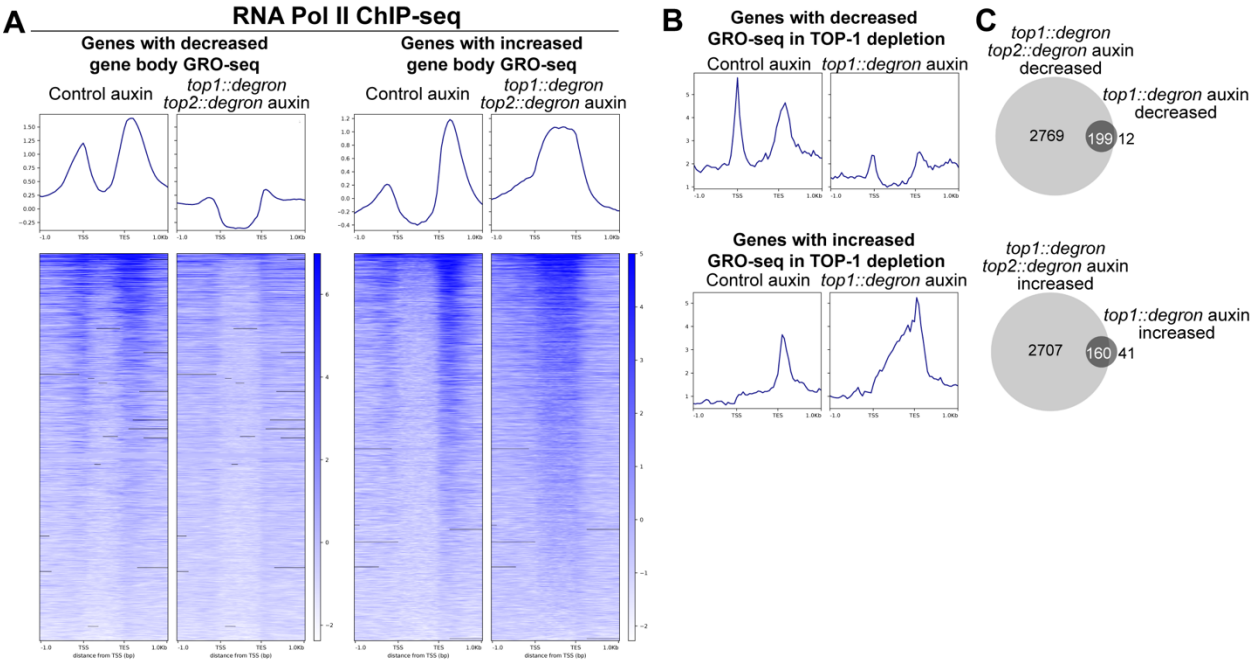

Supplementary Figure 3

A Heatmap showing RNA Pol II ChIP-seq scores for control auxin and *top-1::degron,top-2::degron* auxin. Genes with significant (pvalue <0.05) decreased gene body GRO-seq are on the left and genes with increased gene body GRO-seq are on the right.

B Average GRO-seq scores in control and *top-1::degron* auxin across genes with decreased and increased GRO-seq levels upon TOP-1 depletion.

C Overlap between genes with decreased and increased GRO-seq levels in *top-1::degron* auxin and *top-1::degron,top-2::degron* auxin.

Supplementary Figure 4

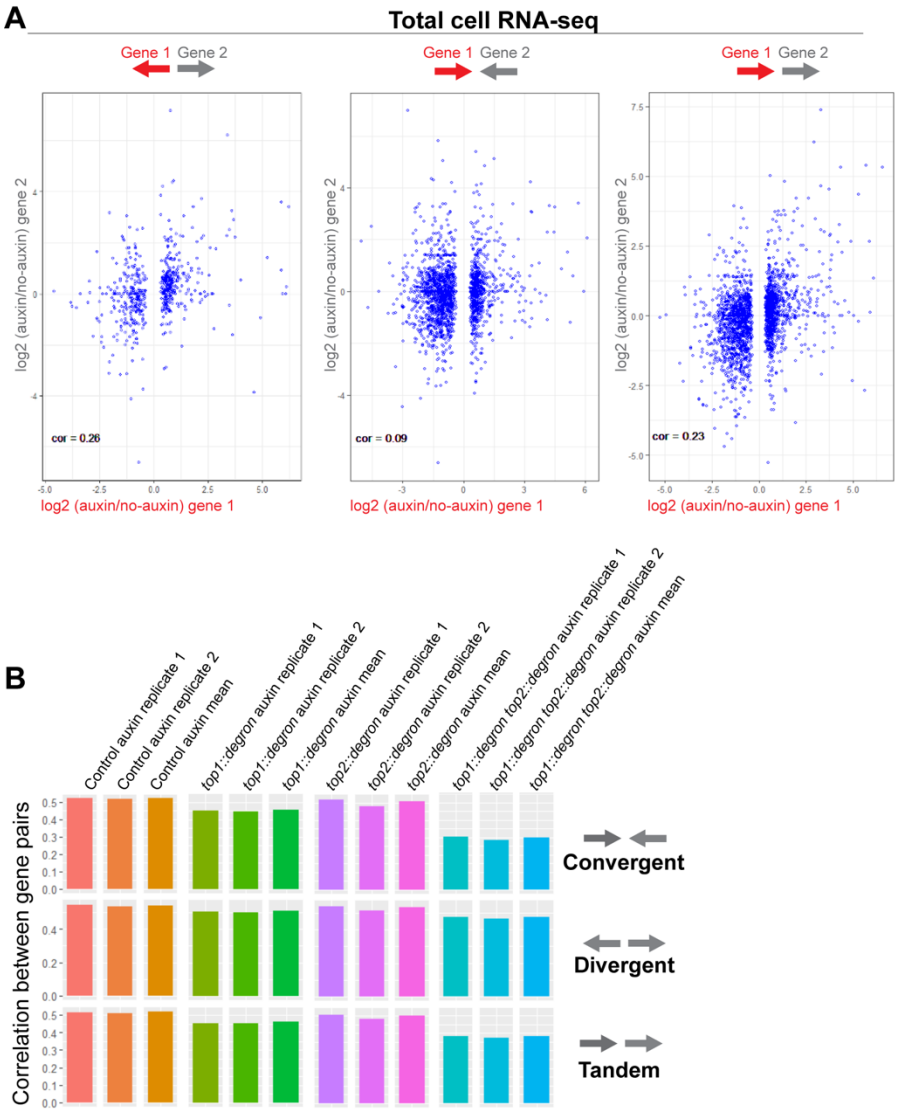

Supplementary Figure 4

A Scatter plot showing log2-fold changes in total cellular RNA-seq between the *top-1::degron,top-2::degron* auxin and no-auxin samples for gene pairs with different orientations.

B Kendal correlations between GRO-seq TPM values of gene pairs with different orientations are shown for control, TOP-1 depletion, TOP-2 depletion and TOP-1/TOP-2 depletion. Values for replicates and average are included.

Supplementary Figure 5

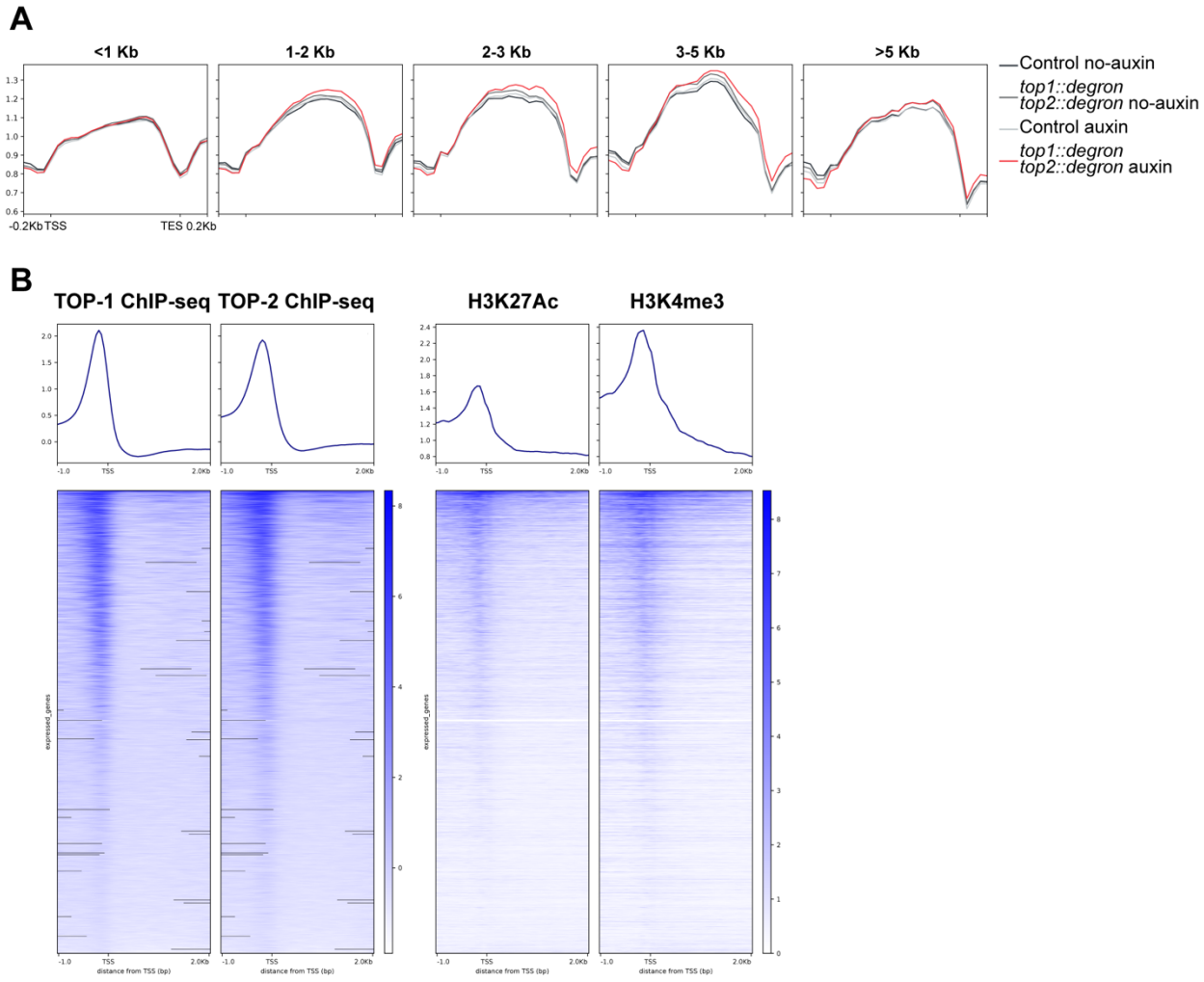

Supplementary Figure 5

A Average H3K36me3 scores in controls (black and gray) and TOP-1/TOP-2 depletion (red) are plotted across genes grouped based on their length into five categories: <1 Kb, 1-2 Kb, 2-3 Kb, 3-5 Kb and >5 Kb.

B Heatmap showing TOP-1 and TOP-2 ChIP-seq scores (data from Morao et al, 2022), and H3K27Ac and H3K4me3 Cut & Tag signal across promoters of expressed genes. Signal in auxin control is shown. Average plots controls are included at the top.

Table S1. List of the *C. elegans* strains used in this study

strain name	***short name***	***short description***	***strain genotype***	***Source***
ERC83	SS01	*top-2::degron::GFP* at endogenous location in the CA1200 strain.	ers55[top-2::degron::GFP] II; ieSi57 [eft-3p::TIR1::mRuby::unc-54 3'UTR + Cbr-unc-119(+)] II	Morao *et al*, 2022
ERC84	AM05	*top-1::degron::GFP* at endogenous location in the CA1200 strain.	ers56[top-1::degron::GFP] I; ieSi57 [eft-3p::TIR1::mRuby::unc-54 3'UTR + Cbr-unc-119(+)] II	Morao *et al*, 2022
		top-1::degron::GFP at endogenous location, *top-2::degron::GFP* at endogenous location in the CA1200 strain.	ers56[top-1::degron::GFP] I; ers55[top-2::degron::GFP] II; ieSi57 [eft-3p::TIR1::mRuby::unc-54 3'UTR + Cbr-unc-119(+)] II	Morao *et al*, 2022
CA1200		Single copy transgene inserted into chromosome II (oxTi179) expressing modified Arabidopsis thaliana TIR1 tagged with mRuby in the soma	ieSi57 [eft-3p::TIR1::mRuby::unc-54 3'UTR + Cbr-unc-119(+)] II	CGC

Table S2. List of the antibodies used in this study

Target	**Antibody**	**Antibody information**
H3K4me3	Active Motif 61979	Mouse monoclonal
H3K27Ac	Epicypher 130045	Mouse monoclonal
H3K36me3	Abcam 9050	Rabbit polyclonal
RNA Pol-II	05-952-I-100UG	Mouse monoclonal
H3K27me3	Diagenode C15410195	Rabbit polyclonal